Microstructure and tribological properties of titanium matrix nanocomposites through powder metallurgy using graphene oxide nanosheets enhanced copper powders and spark plasma sintering

N. Tian [a], L.L. Dong [b, c*], H.L. Wang [a*], Y.Q. Fu [d], W.T. Huo [b], Y. Liu [b], J.S. Yu [c], Y.S. Zhang [e]

[a] School of Materials Science and Engineering, Xi'an Shiyou University, Xi'an 710065, PR China

[b] Advanced Materials Research Central, Northwest Institute for Nonferrous Metal Research, Xi'an 710016, PR China

[c] School of Materials Science and Engineering, Northeastern University, Shenyang 110819, PR China

[d] Faculty of Engineering and Environment, Northumbria University, Newcastle upon Tyne, NE1 8ST, UK

[e] Xi'an Rare Metal Materials Institute Co., Ltd, Xi'an, 710016, PR China

ABSTRACT:

Titanium alloys have been applied for many lightweight structural components in the fields of aerospace, automobiles and biomedical implants owing to their light-weight, good mechanical properties and biocompatibility. However, poor tribological performance often restricts their wide-range applications. In this study, we

* Corresponding author:
E-mail: donglong1027@163.com (L.L. Dong), wanghl@xsyu.edu.cn (H.L. Wang)

synthesized Cu modified Ti-6Al-4V (TC4) powders with various Cu contents (1, 3, 5, 10 wt%), which was further strengthened with 0.3 wt% graphene oxide nanosheets (GONs) using a powder metallurgy technology. These composite powders were then synthesized into titanium matrix composites using spark plasma sintering. Effects of Cu contents on microstructure evolution, phase composition and tribological properties of Ti matrix composites were systematically investigated. The synthesized composites were consisted of α-Ti, β-Ti, Ti_2Cu, *in-situ*-formed TiC and remained GONs, and showed better tribological properties than those of TC4 alloy. The average coefficient of friction was reduced from 0.168 to a minimum value of 0.120 as the copper content increased from 0 to 3 wt%, meanwhile the wear volume loss was reduced by 49.3%. Whereas further increasing copper contents resulted in the increases of both coefficients of friction and wear volume loss. These improvements are mainly attributed to the strengthening effects by nanoscaled Ti-Cu intermetallics and TiC@GONs structure, as well as the self-lubricating effect of GONs. Compared with traditional surface modification processes, the new method proposed in this work is cost-effective and promising for improving the tribological performance of titanium alloys in industry applications.

Keywords: Ti matrix composites, Tribological properties, Microstructure, Powder modification, Spark plasma sintering

1. Introduction

Titanium and its alloys are ideal materials for petrochemical and medical applications due to their attractive properties such as light weight, high specific

strength, and good corrosion resistance and antibacterial properties [1-3]. However, application of new types of high-performance structural materials normally requires not only their strength and toughness, but also their good wear resistance. The poor wear resistance of titanium materials influences not only their surface appearance, but also their sensitivity of crack initiation and shortening of the part life due to early failure under complex loads or environments. To improve the comprehensive mechanical properties especially the tribological properties of titanium materials, considerable research has been focused on the applications of various surface modification and strengthening strategies [4-6]. So far, introduction of various nanoscale ceramic particles (TiC, TiB, Al_2O_3, SiC) into Ti matrix has gained extensive attention [7-10].

To our knowledge, graphene and its derivatives have been demonstrated to be effective for reinforcing metal matrix composites [11-14] owing to their unique 2D structures and overall high performances. However, there are always concerns for the uniform dispersion of graphene and the resulting good enhancement in mechanical properties, especially the strength of the composites. Chu et al. [15] reported that the yield strength of the graphene/copper composites was increased by 37% reaching 300 MPa compared to pure copper when 8 vol.% graphene was added. Compared with Al, Wu et al. [16] found that the tensile strength of the graphene reinforced Al composites was increased by 73.9% meanwhile the ductility maintained more than 10%. Previously, Dong et al [17] showed that using spark plasma sintering (SPS) technique, addition of only 0.3wt.% of GONs into Ti matrix composites (TiMC) led to the yield

strength and ultimate tensile strength of the composites increased by 7.44% and 9.65%, respectively. Zhang's group fabricated Ni coated graphene nanoplates reinforced Ti composites using mechanical agitation and SPS, and achieved a strength of 793 MPa, which is ~ 40% higher than that of monolithic Ti matrix [18]. However, among all these studies, few of them have been focused on the tribological behavior of graphene/Ti composites. Ti-6Al-4V alloys is the most extensively used Ti alloy among all the Ti materials, however, they have a poor wear resistance, thus limiting their applications where wear resistance is essential.

This study aims to explore the relationship between tribological performance and composition as well as microstructure of graphene/Ti composites, and to reveal the fundamental mechanisms on the damage of the composites resulted from wear. To achieve this, copper powders with different contents (1, 3, 5, 10 wt%) and 0.3% GONs were synergistically added into Ti-6Al-4V (TC4) matrix using a novel powder modification technology and then the composites were synthesized using SPS in order to improve their tribological properties. The copper was chosen as an alloying element to modify the TC4 powders because it is a β-stabilizing element. According to the equilibrium phase diagram of Ti-Cu binary alloys, Ti–Cu alloys with a low Cu content consists of a matrix of α-Ti and precipitates of Ti_2Cu intermetallic compounds [19]. It was reported that the Ti alloys with appropriate Cu concentrations show good biocompatibility [20], corrosion resistance [21, 22] and mechanical properties [23]. For examples, Kikuchi et al. reported that the mechanical properties of cast Ti-*x*Cu (*x*= 0.5-10 wt%) alloy have been significantly improved compared with those of pure

Ti (e.g., tensile strength and yield strength have been increased up to 30% and 40%, respectively [23].

The SPS was used because of its advantages such as short sintering time, fast heating rate, controllable structure, uniform temperature and simple operation, which can achieve uniform microstructure and high density of the sintered materials by inhibiting their grain growths [24, 25]. The microstructure and wear behavior of the composites were systematically characterized, and the wear mechanisms were discussed. The Ti matrix composites showed the highest hardness with a value of 411 HV with 5 wt.% copper content, which is ~25% higher than that of the TC4 alloy (330 HV). The composites showed the lowest coefficients of friction (0.12) and the wear volume loss (0.155 mm^3) among the alloys and composites studied in the present work. The improvement of tribological properties is due to the strengthening by the nanoscale precipitates (Ti_2Cu and TiC) at high temperatures, self-lubricating effect introduced by the pulled-out GONs from the composites, the fragileness of the brittle TiC@GONs structure, as well as the enhanced heat conduction resulted from the high heat conductivity of the preserved elemental copper and graphene. The GONs-*x*Cu@TC4 composites with a good wear resistance developed in this work has their promising applications in the field of brake discs and aerospace.

2 Experimental

2.1 Raw Materials

Ti-6Al-4V spherical powders with an average particle size of 15-53 μm were used as the matrix material, and they were purchased from Xi'an Sino-Euro Materials

Technologies Co., Ltd., China. **Figure 1a** shows a scanning electron microscope (SEM, JEOL JSM-6700F) image, and their chemical composition is listed in **Table 1**. The particle size of the TC4 powders conforms to a normal distribution with an average value of 37 μm (inset in **Figure 1a**). The wide distribution of the particle size is beneficial for the full densification of the powders as the fine particles can fill the spaces in the triangle intersections of coarse particles during the following SPS process [26]. The average size of the Cu powders is 48 μm, and they were supplied by Beijing Xin Rong Yuan Technology Co., Ltd., China. An SEM image of the pure Cu powders shown in **Figure 1b** reveals their flower-like and flocculent patterns which are composed of fine copper particles. GONs with diameters of 0.5~5 um and thicknesses of 1~3 nm were purchased from XFNANO Technology Co., Ltd., China. A transmission electron microscope (TEM) was used to characterize the GONs. For the TEM observation, the GON nanopowders were firstly dispersed into ethanol and then drop casted onto an amorphous carbon coated copper grid [27]. An TEM image in **Figure 1c** shows a crumpled and thin-layered sheet structure, which is the typical morphology of graphene oxides. A high-resolution TEM (HRTEM) image shown in **Figure 1d** presents that the GONs have a few layer structure. The selected area electron diffraction (SAED) pattern of the GONs displays two diffraction rings, corresponding to $(10\bar{1}1)$ and $(11\bar{2}0)$ planes of the graphene (**Figure 1e**). **Table 1** lists chemical compositions of both the TC4 and Cu powders.

Table 1. Chemical composition of Ti-6Al-4V and copper powders (wt %).

Materials	Al	V	Fe	C	N	O	H	Cu	Ti

Ti6Al4V	6.17	4.23	0.17	0.008	<0.003	0.10	0.0048	-	Bal.
Cu	-	-	-	-	-	0.012	0.002	Bal.	-

2.2 Fabrication of the GONs-*x*Cu@TC4 composites

2.2.1 Preparation of mixture powders

In order to disperse the copper powders and GONs uniformly in the TC4 powders, a two-step shift-speed ball milling process was adopted to prepare mixture powders. (1) The mixed powders of copper and TC4 were ball-milled for 2 hours in an Ar atmosphere at a speed of 300 r/min with a ball ratio of 3:1 in the same direction. (2) Based on the previous study [17], we have chosen 0.3 wt% GONs to be added into the Cu modified TC4 powders using a low-energy ball milling, with a speed of 150 r/min for another 3 hrs. The aim is to coat the GONs uniformly onto the composite powder surfaces. Five types of mixing powders were prepared, i.e., mixtures with copper contents of 1 wt%, 3 wt%, 5 wt%, 10 wt% and a mixture without copper. **Figure 1f** shows an SEM image of the composite powders after two-step ball milling. Clearly the TC4 powders are slightly deformed. Whereas copper powders are severely deformed, i.e. their shapes are transformed into a smaller flake-shape, and they are tightly attached to the surfaces of TC4 powders. The GONs are uniformly dispersed onto the surface of TC4, which is clearly indicated by the energy dispersion X-ray spectrum (EDS) (**Figure 1g**).

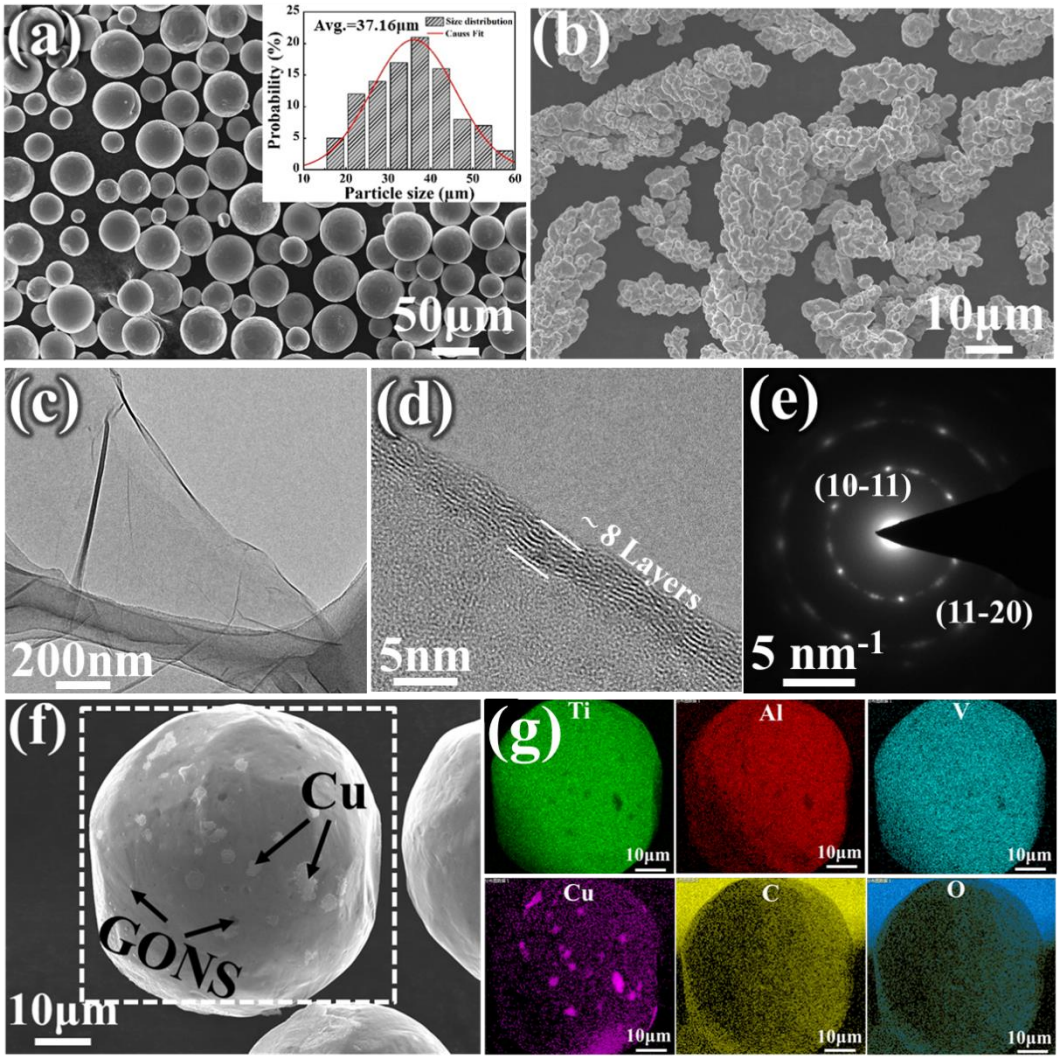

Figure 1. (a) SEM of raw TC4 powders and (b) copper powders; (c) TEM, (d) HRTEM images of GONs and (e) the corresponding SAED pattern; (f) GONs-1Cu/TC4 composites powders; (g) EDS mapping images of Ti, Al, V, Cu, C, O elements, respectively.

2.2.2 Fabrication of Ti matrix composites

SPS is one of the best sintering processes for preparing metal matrix composites (MMCs) owing to its high efficiency. **Figure 2** shows the powder metallurgy and SPS processes for fabrication of TiMCs in this work. The mixed powders were loaded into

a graphite grinder with an internal diameter of 60 mm and an external diameter of 100 mm. The graphite paper with a thickness of 1~2 mm were placed around the powders to prevent the reaction and bonding of TC4 powder with the graphite mold.

The vacuum of SPS furnace was maintained at ~10^{-2}~10^{-3} Pa during sintering. The holding pressure, heating rate, and sintering temperature were 45 MPa, 100 ºC/min, 1000 ºC, respectively. There was a temperature monitoring hole with a diameter of 10 mm in the middle of the graphite mold. During the sintering, the temperature was measured using an infrared camera, which was positioned at about 5 mm from the sample center. After sintering for about 5 minutes, the samples were cooled down with the furnace. Pure TC4 alloy and GONs/TC4 composites without Cu were also sintered under the same conditions for comparisons. The selection of detailed sintering parameters was described in a previous study [17]. For simplification, hereafter the as-sintered TiMCs with different Cu contents were named as GONs-*x*Cu/TC4 composites (*x*=0, 1, 3, 5 and 10 wt%). The relative densities of these sintered Ti composites were determined using the Archimedes' method [11], and the obtained results are listed in Table 1. Clearly all the composites show a higher relative density than that of pure TC4.

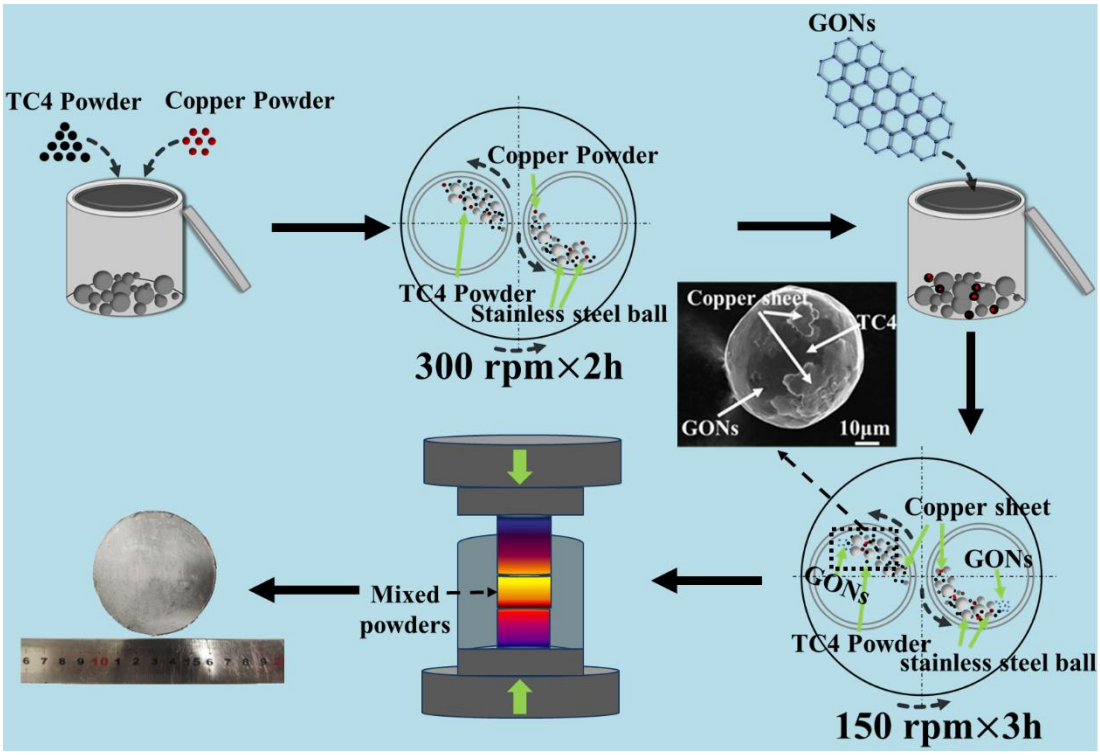

Figure 2. Schematic illustrations of fabrication procedures for the GONs-Cu/TC4 composites using powder modification and SPS.

Table 1. The theoretical density, measured density and relative density of fabricated Ti matrix composites.

Materials	Theoretical density (g/cm^3)	Measured density (g/cm^3)	Relative density (%)
TC4	4.510	4.407±0.009	97.72
GONs/TC4	4.494	4.405±0.005	98.02
GONs-1Cu/TC4	4.516	4.439±0.008	98.29
GONs-3Cu/TC4	4.560	4.486±0.010	98.38
GONs-5Cu/TC4	4.603	4.513±0.013	98.04
GONs-10Cu/TC4	4.707	4.616±0.015	98.07

2.2.3 Wear and hardness tests

Before testing hardness and wear behavior of the composites, all the sintered

samples were polished to 2000 grits, and then ultrasonically cleaned with acetone and ethanol. Vickers hardness was tested using an HVS-1000 machine with a load of 3 N and a dwell time of 15 s at 10 different locations. Then the average value was obtained to represent the hardness of the sample.

The wear behavior of the composites was tested using a MS-T3001 rotary friction testing machine (Lanzhou Huahui Instrument Technology Co.,) by dry sliding at room temperature in air. A Si_3N_4 ball with a diameter of 4 mm was used as the counterpart. The test was conducted with the normal load of 50 N, the rotary speed of 400 r/min and the rotation radius of 3 mm for 120 min. The friction coefficients of the samples were recorded automatically. Profiles of the worn surfaces were measured using a MicroXAM 3D surface profilometer system in order to determine the wear volume loss. The morphologies of the worn surface with different wear conditions were characterized using the SEM.

2.2.4 Microstructures of composite materials

Microstructures of the composites and the prepared powders were characterized using the SEM. Before observation, the Ti matrix composites were polished with 2000 grits of silicon carbide sandpaper, cleaned ultrasonically in an alcohol solution and then polished with alumina polishing solution. After that, the surface of the composites was etched using a solution of hydrofluoric acid, nitric acid and water, with ratios of 1:3:5 (vol.%). The phases in the composites were identified using X-ray diffraction (XRD, Bruker D8 ADVANCE) with Cu-K_α radiation and a scanning rate

of 10°/min.

Raman spectroscopy was used to investigate defects in the GONs and presence of TiC, and the scan range of laser beam was from 300 to 3000 cm^{-1}. The tests were performed at room temperature using a Laser Raman Spectrometer (LabRAM HR Ecolution) with an excitation wavelength of 532 nm.

An X-ray photoelectron spectroscope (XPS, Thermo SCIENTIFIC ESCALAB 250Xi, Al-K_α source) with an analysis chamber pressure of 4×10^{-8} Pa, was applied to investigate the chemical valences of surface elements of sintered Ti matrix composites.

3 Results and discussions

3.1 Microstructure Evolution and Phase Analysis

SEM images of the sintered GONs/TC4 composites with various copper contents are shown in **Figure 3**. The monolithic TC4 alloy without the addition of copper and GONs has a typical Widmanstätten lamellar microstructure (**Figure 3a**), consisting of the lath-shaped α phase, the α phase at grain boundaries (α_G) and the intergranular β phase (**Figure 3a$_1$**) The size of the primary β grains is much larger (~450 um) than that of the raw TC4 powder (~38 um, **Figure 1a**), which is due to the slow cooling process from the β transformation temperature [28]. However, owing to the introduction of Cu and GONs, the grain size of primary β phases in **Figures 3b~3e** is much smaller than that of the TC4 monolithic alloy (**Figure 3a**), which is beneficial to the enhancement of their mechanical properties. When the content of copper reaches

10 wt.% in the composites, the primary β grain boundary disappears as shown in **Figure 3e**.

Besides the α phase and the β phase, the unreacted GONs, the *in-situ* formed TiC particles or layers (**Figure 3b$_1$**) and the nanoscale Ti_2Cu precipitates co-exist in the composites as shown in **Figures 3b~3e**. The EDS mapping analysis in Figure 3d$_1$ shows that the Cu is preferred to distribute around the β phase because the Cu is a β stabilizing element. C element is relatively homogeneously distributed inside the Ti matrix without obvious agglomerations. The formation of TiC is attributed to the initiative reactions between C and Ti matrix [29], which is beneficial to the interfacial strength and tribological properties. The presence of Ti_2Cu is evidenced by the energy dispersion spectrum (EDS) results (**Figure 3b$_2$, inset**). The microstructure near point 1 in **Figure 3b$_2$** consists of Ti (50.51 at.%) and Cu (27.19 at%), indicating that the Ti_2Cu phase was nucleated and grown during the SPS process.

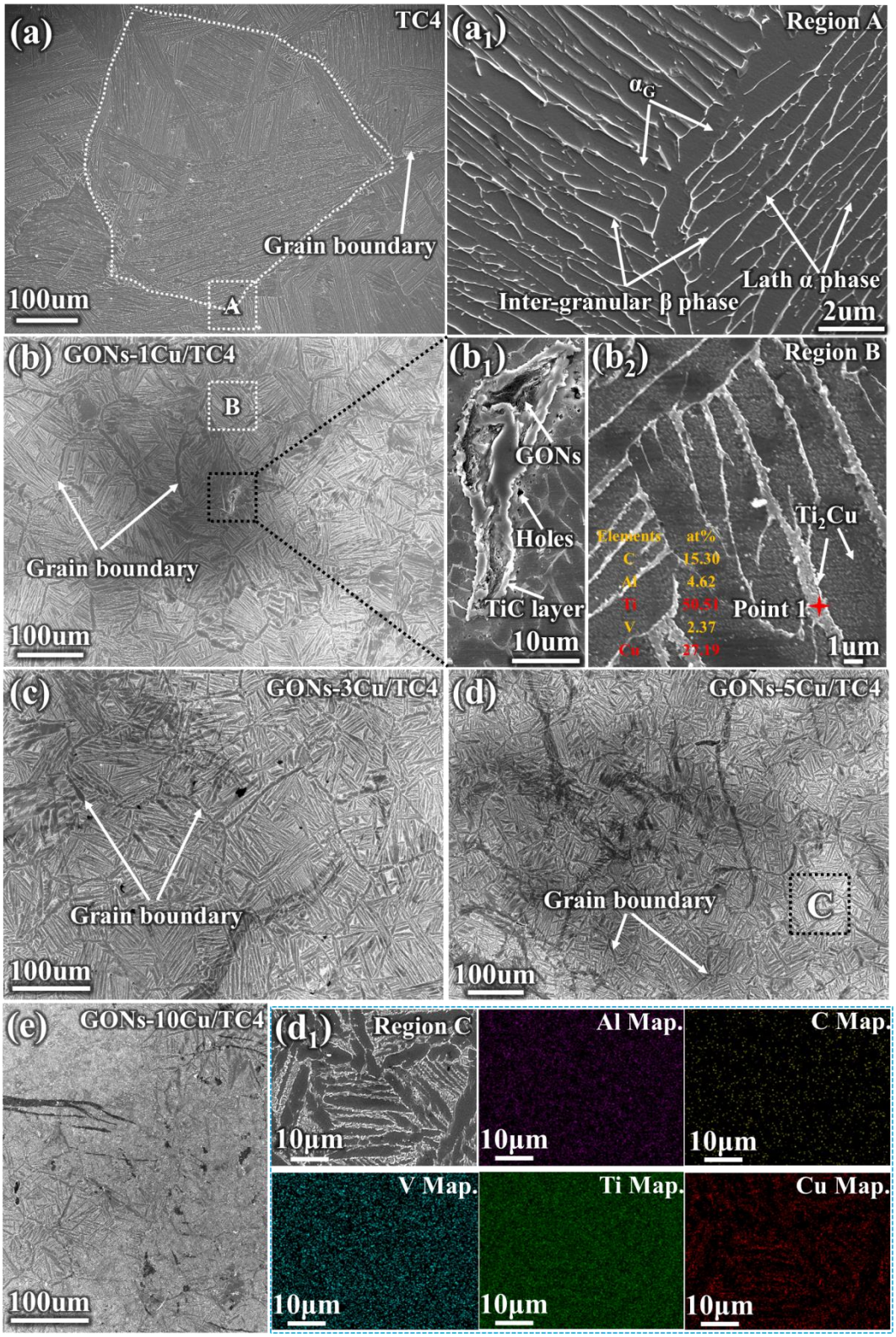

Figure 3. SEM images of GONs-*x*Cu/TC4 composites with different Cu contents. (a) ~ (a_1) pure TC4; (b)~(b_2) GONs-1Cu/TC4; (c) GONs-3Cu/TC4; (d) GONs-5Cu/TC4; (e) GONs-10Cu/TC4; (a_1) and (b_1)~(b_2) are enlarged images of corresponding marked

region in Figure (a) and Figure (b), respectively. (d_1) EDS mapping analysis of the marked region C in Figure (d).

To further verify the phases of the sintered composites, XRD analysis was carried out and the results are shown in **Figures 4a** and **4b**. A peak at ~ 39.49° (PDF # 15-717) corresponding to the (103) of Ti_2Cu is identified in the XRD results and its intensity increases significantly with the addition of copper. Meanwhile, Cu, β-Ti phase, TiC and GONs could not be detected by XRD for all the composites and TC4 alloy. The XRD results indicate that the main phase is α-Ti and the secondary phase in the composites is mainly Ti_2Cu. No elemental copper is found in the composites because the reactions between copper and titanium during sintering result in the formation of Ti_2Cu. Although other phases, i.e., GONs, TiC and β-Ti phase are observed by SEM, their contents are out of the detecting limit of the XRD instrument used in the present work [30].

According to the phase diagram of titanium-graphite, TiC is the only type of intermetallics that could form in the Ti-C system. Although the composite is a multi-elements system containing Ti, Al, V, Cu, C and O, the mixing of C, Cu with the matrix TC4 is not at an atomic level but at a microscale level. Taking into account the short sintering time of SPS, the local environment of Ti-C or Ti-Cu could be considered as binary systems. At the sintering temperature of 1273 K, the change of Gibbs energy is estimated to be -84.4 kJ/mol for the following reaction [31, 32]:

$$Ti+C=TiC \qquad \triangle G_1=-92400+6.275T \text{ J/mol} \qquad (1)$$

Hence, TiC is resulted from the spontaneous reaction between the matrix Ti and

the carbon from the GONs [29]. Similarly, Ti_2Cu is the preferable phase when the content of Cu is less than 33.3 at.%, according to the binary phase diagram of Ti-Cu. The change of Gibbs energy can be estimated as -6.2 kJ/mol at 1273 K for the following reaction [31, 32]:

$$2Ti+Cu=Ti_2Cu \qquad \triangle G_2=-12131+4.688T \text{ J/mol} \qquad (2)$$

which also indicates that the formation of Ti_2Cu is spontaneous.

To further verify the existence of TiC intermetallics and GONs in the composites, Raman and XPS spectroscopies were used. The Raman spectra of the raw GONs and the TiMCs are shown in **Figure 4c** and the main peaks are listed in **Table 2**. The characteristic Raman peaks for graphene are similar to those of the composites, i.e., the G band at ~ 1580 cm^{-1} is originated from the in-plane vibration of sp^2 carbon atoms, the D band at ~ 1350 cm^{-1} corresponds to the doubly resonant disorder-induced mode related to the defects, and the 2D band at ~ 2700 cm^{-1} represents the feature of graphene [27, 33]. Similar characteristic bands between the composites and the raw GONs confirm that the GONs is retained in the TiMCs. It is also noticed that the I_D/I_G values for all the composites are significantly higher than the corresponding value for the GONs. Since I_D increases with the density of defects [27], the increase of the I_D/I_G value for the composites suggests the introduction of defects into the GONs during the ball milling or sintering process.

Besides the characteristic peaks of graphene in the composites, two additional Raman peaks located at ~ 418 cm^{-1} and ~ 605 cm^{-1} suggest the presence of TiC [34]. Further investigation using the XPS was carried out, and **Figure 4d** and **Figure 4e**

show that the peaks at 454.6 eV and 460.2 eV correspond to the binding energy of the Ti-C bond, which verifies the existence of the TiC intermetallics. In addition to the main peaks of Ti located at 453.8 eV for $Ti_{2p}^{3/2}$ and 459.95 eV for $Ti_{2p}^{1/2}$ in the XPS spectrum, peaks at 932.5 eV for $Cu_{2p}^{1/2}$ and 952.4 eV for $Cu_{2p}^{3/2}$ as shown in **Figure 4f** correspond to the binding energy of the Cu-O bond. XPS analysis proves the formation of the Cu-O bonds in the composites, which is helpful for improving the interfacial bonding strength between the Cu and GONs [35].

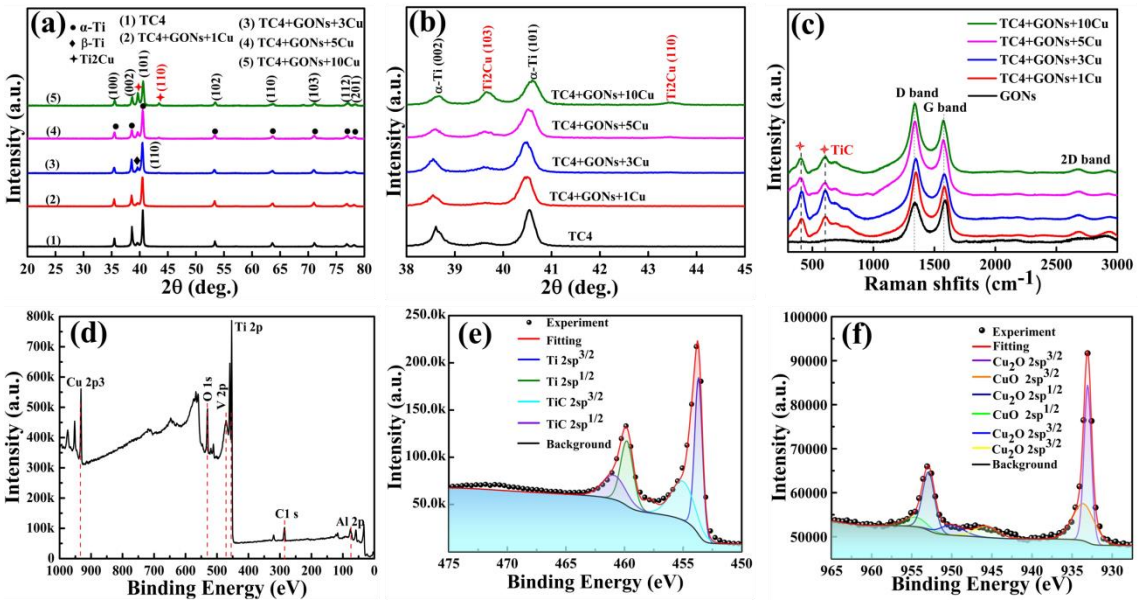

Figure 4. XRD, Raman and XPS analysis results for GONs-*x*Cu/TC4 composites: (a) XRD patterns; (b) An enlarged XRD patterns at 2θ=38~45° in Figure (a); (c) Raman spectra of composites; (d) XPS survey spectra of GONs-5Cu/TC4 composites; High resolution XPS spectrum of Ti_{2p}; High resolution XPS spectrum of (e) Ti_{2p} and (f) Cu_{2p}, respectively.

Table 2. The detailed Raman spectra results of the sintered GONs-*x*Cu/TC4 composites.

Materials	D band	G band	2D band	I_D/I_G
GONs	1351.28	1587.31	2695.91	0.95
GONs-1Cu/TC4	1346.64	1581.16	2679.29	1.23
GONs-3Cu/TC4	1349.62	1581.15	2685.78	1.28
GONs-5Cu/TC4	1348.48	1579.44	2685.44	1.30
GONs-10Cu/TC4	1346.13	1577.16	2679.94	1.31

3.2 Tribological properties

Figure 5a presents the effect of Cu contents on the hardness of sintered Ti matrix composites. The Vickers hardness of the composites increases from 330 HV to 411 HV when the content of Cu is increased from 0 to 5 wt.%. According to the characterization of the microstructure aforementioned, the hardness enhancement of the composites is attributed to the strengthening effect due to the smaller grain sizes, the fine second phases of Ti_2Cu, TiC and the preserved GONs, especially a large number of Ti_2Cu precipitates. Further addition of Cu results in a slight decrease of the hardness, due to the softening effect induced by the elemental copper which is not reacted with the titanium matrix during the short sintering time of SPS.

The coefficients of friction (COFs) vary with the sliding time during the wear tests as shown in **Figure 5b**. The friction experiences an unstable initial stage for all the samples. The duration of this unstable stage is much longer for the TC4 alloy (~65 min) and the GONs-1Cu/TC4 composite (~50 min) than that for the composite with the content of copper above 1 wt.% (~10 min). After the running-in stage, the COF

curves of the samples stabilize gradually. The initial fluctuation of the COFs is due to the “break-in” or “running-in” period and an unstable surface roughness of the specimens during the initial sliding [36, 37]. However, the COFs of the GONs/TC4 composites are reduced after ~ 40 min, which is attributed to the presence of GONs, whose delamination can induce a lubrication effect during the sliding process (inset, Figure 8b_1).

The average COFs versus the copper content of the composites are plotted in **Figure 5c**. The COF of the composite with 3 wt.% of Cu is the minimum among the five types of samples. The increase of deviation for the Cu content from 3 wt.% accompanies the increase of the COFs. The wear depth and width were determined from the cross sectional profiles of the wear scars, and the results are shown in **Figure 6.** They show similar trends to the COFs, i.e., the minimum values are around 3wt.% of Cu as shown in **Figure 5d**. The variation trends of the wear volume losses with the copper content (**Figure 5e**) are similar to those of the COFs. Compared to that of the pure TC4 alloy, the wear volume losses of the composites with GONs and Cu are significantly lower. In particular, the minimum wear volume loss is found in the composite with a copper content of 3 wt.%, and the wear volume loss of this kind of composite is about half the value of the monolithic TC4 alloy. These reveal that the addition of Cu and GONs can remarkably improve the wear resistance properties compared with the unreinforced matrix alloy. The wear volume loss was also evaluated based on the 3D morphology of the wear tracks (**Figure 6**). The wear volume loss as well as the average COFs are listed in **Table 3**.

Table 3. The wear properties of the sintered GONs-*x*Cu/TC4 composites.

Wear properties	Cu contents					
	TC4	0 wt.%	1 wt.%	3 wt.%	5 wt.%	10 wt.%
Average COFs	0.1680±0.011	0.1389±0.017	0.150±0.012	0.120±0.015	0.130±0.01	0.140±0.015
Wear width (μm)	3533±45	3190±28	2895±30	2953±35	3341±38	3353±45
Wear height (μm)	472±5	439±6	352±7	335±8	371±9	468±5
Wear volume loss (mm^3)	0.306±0.015	0.168 ±0.008	0.176±0.009	0.155±0.01	0.202±0.012	0.230±0.008

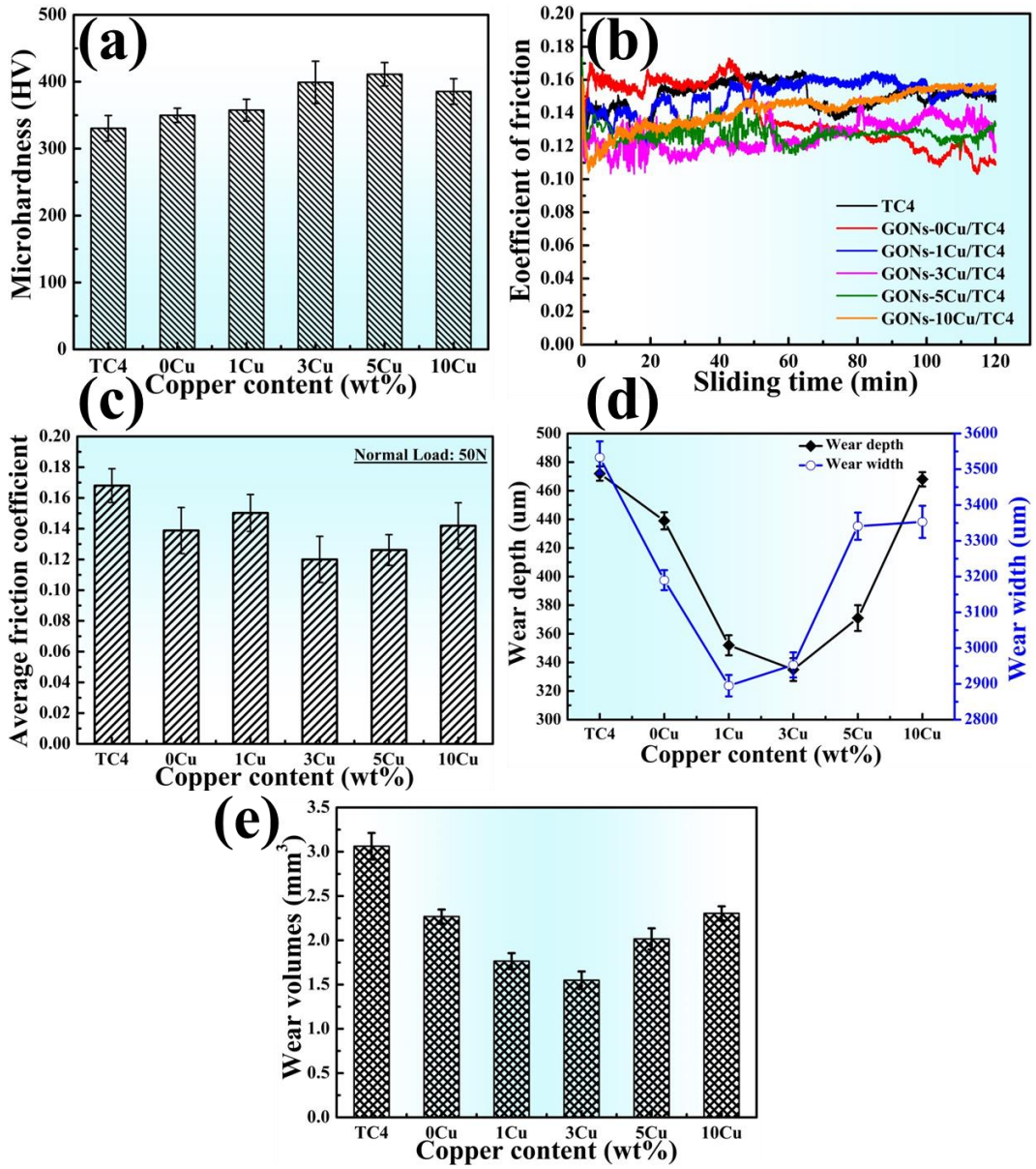

Figure 5. (a) Hardness of sintered TiMCs samples, (b) Variations of friction

coefficient of GONs-*x*Cu/TC4 composites under a normal load of 50 N, (c) The average friction coefficients of all samples, (d) Wear depth and the maximum wear depth of scars for sintered composites, and (e) Wear volumes loss of different samples, respectively.

The wear debris at the surface of the wear scars were examined using SEM and EDS, and the results are shown in **Figure 7**. The shape of the wear debris changes with the increase of copper content in the composites. On the specimen surface of the TC4 alloy, there exists two types of wear debris, i.e., the plate-like debris with an average size of ~80 μm and the fragments of fine particles with an average size of ~10 μm (**Figure 7a**). With the addition of copper and GONs into the TC4 matrix, the plate-like debris are still the main feature, but the number of the fine particle fragments is reduced drastically and almost becomes zero when the copper content is 10 wt.%. The debris surfaces of the composites with copper contents of 5 wt.% (**Figure 7d$_1$**) and 10 wt.% (**Figure 7e$_2$**) show deep grooves, indicating significant ploughing features during sliding wear. It was also noticed that the oxygen content in the wear debris of the composites is lower than the corresponding value of the TC4 alloy as shown in the EDS results in **Figure 7**.

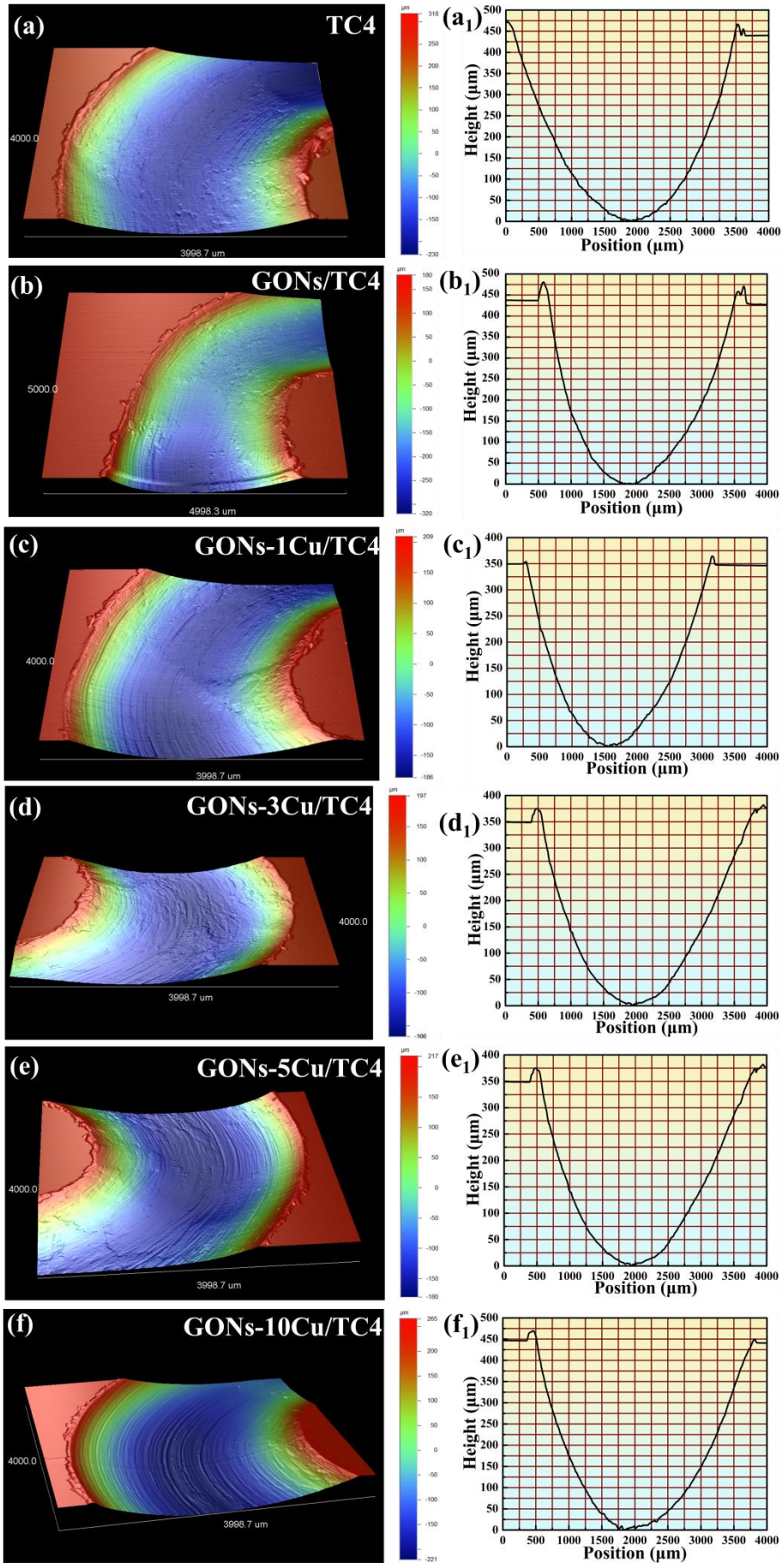
(a)
TC4
4000.0
3998.7 um
(a1)
Height (μm)
Position (μm)
(b)
GONs/TC4
5000.0
4998.3 um
(b1)
Height (μm)
Position (μm)
(c)
GONs-1Cu/TC4
4000.0
3998.7 um
(c1)
Height (μm)
Position (μm)
(d)
GONs-3Cu/TC4
4000.0
3998.7 um
(d1)
Height (μm)
Position (μm)
(e)
GONs-5Cu/TC4
4000.0
3998.7 um
(e1)
Height (μm)
Position (μm)
(f)
GONs-10Cu/TC4
4000.0
3998.7 um
(f1)
Height (μm)
Position (μm)

1

Figure 6. (a ~ f) Surface 3D morphologies of the wear scars for sintered composites with various Cu contents and (a_1, b_1, c_1, d_1, e_1 and f_1) corresponding 2D cross-section profiles of wear tracks, respectively.

The corresponding worn surfaces and the wear debris were also examined using the SEM and EDS. The results are shown in **Figure 8** and the obtained compositions are listed in **Table 4**. The amount of wear debris on the worn surface decreases with increasing copper content in the composites. The worn surface on the samples of the TC4 alloy is consisted of deep grooves and parallel furrows with some detached edges, indicating significant ploughing features during sliding wear. Ploughing or plastic deformation is a typical characteristic of the abrasion and adhesion wear [38]. Elements detected in the grooves are mainly Ti, Al, V and O (Point 1 in **Figure 8a$_1$** and spectrum in **Figure 8f**), and the content of oxygen is as high as 30.21 at.%, indicating significant oxidation of the alloy in the surface layer during the reciprocal wear process.

The grooves on the samples of the composites become gradually smoothened with increasing the copper content. In addition to the elements existed in the grooves on the surface of the TC4 alloy, Si, C and Cu elements are also found on the surface of the composite samples. The element Si is transferred from the Si_3N_4 balls, indicating that the adhesion wear occurs between the composite and Si_3N_4 ceramic ball.

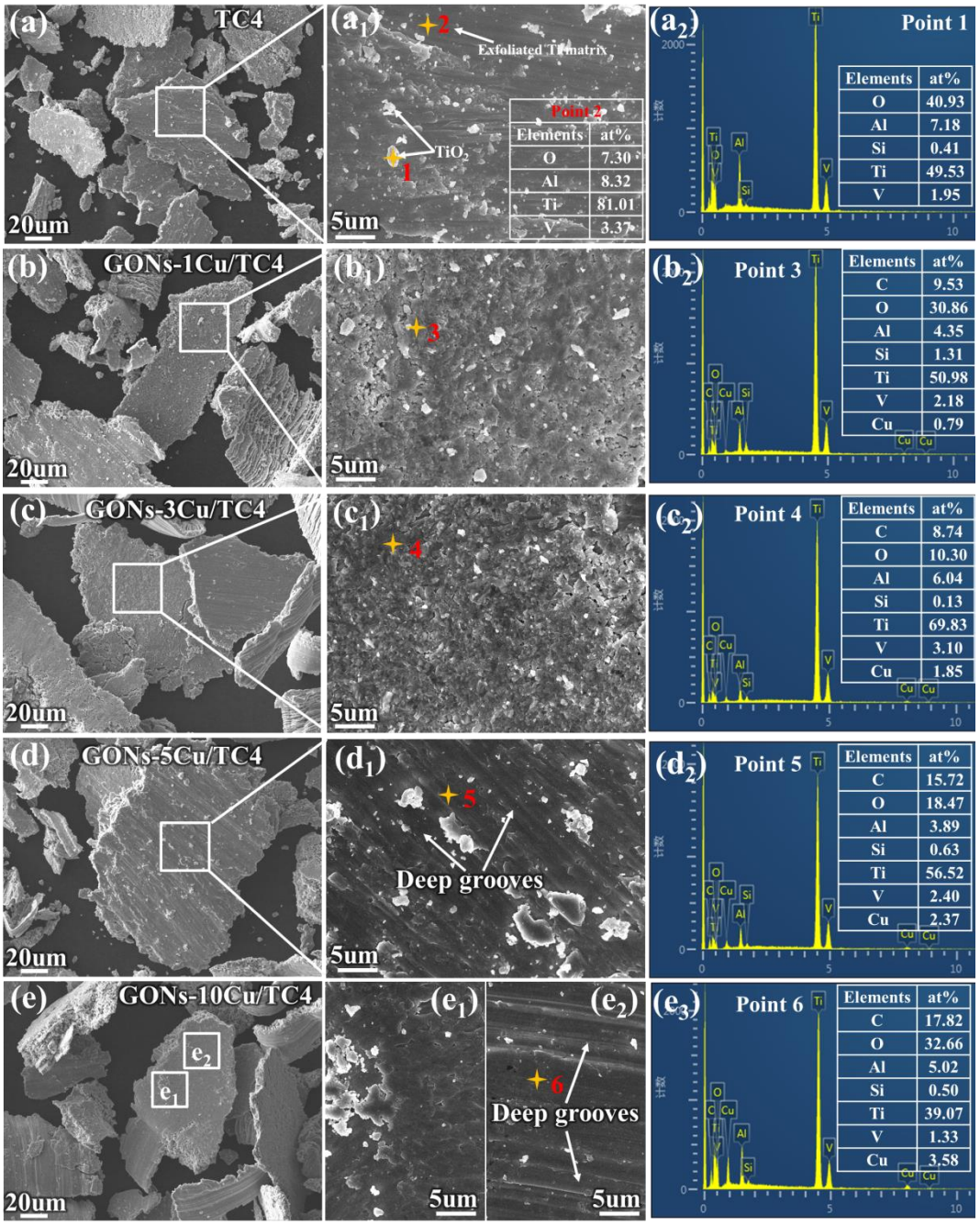

Figure 7. SEM images of wear debris of GONs-*x*Cu/TC4 composites and Si_3N_4 ball frication pair after sliding wear test under 50 N load. (a) TC4, (b) GONs-1Cu/TC4, (c) GONs-3Cu/TC4, (d) GONs-5Cu/TC4, (e) GONs-10Cu/TC4, (a_1)~(e_1) enlarged images of corresponding marked region in Figures (a)~(e) and (a_2)~(e_3) EDS result of points 1, 2, 3, 4, 5 and 6, respectively.

Besides the grooves and the wear debris, delamination phenomena are also observed on the sample surface of the composites (**Figures 8c$_1$, d$_1$ and e$_1$**). At some delaminated regions (**Figure 8d$_1$**), high content of carbon is detected by EDS (**Figure 8f**), revealing the pulling out of the GONs from the interfaces in the composites. Furthermore, microscale voids and cracks are found on the sample surface of composites with the content of copper higher than 3wt.% (**Figures 8d$_1$ and e$_1$**).

According to the aforementioned phenomenon, the wear on the TC4 alloy or the TC4 based composites is a comprehensive mechanical-chemical coupling process. The chemical reactions mainly involve the oxidation of the metals in the alloys or composites. The sliding process of the Si_3N_4 ball on the surface applies a complicated dynamically localized loading onto the sample, and this added load fluctuates continuously with changes of worn morphology, local temperature of sample, and formation of wear debris. Under wear process, the mechanical behavior of the TC4 alloy or the TC4 based composites involves ploughing or plastic deformation, work hardening, local crack initiation and propagation, local welding and pulling out of the GONs.

Generally, the harder or stronger the metallic materials is, the lower the coefficients of friction and the better the tribological properties are [39]. However Ti and its alloys are differnt, i.e., the higher of their strength is, the higher is the coefficients of friction and the poorer of their tribological properties [40]. In this study, we provide a solution for improving the wear resistance of the TC4 based metallic materials by forming the composites via SPS using TC4 powders modified with Cu

and GONs, and we have achieved both high strength and improved tribological properties of Ti matrix composites (**Figure 5**).

A schematic illustration on the tribological behavior and the wear mechanism of the Ti matrix composites is shown in **Figure 9**. After sintering, the Widmanstätten microstructure is formed in the TC4 alloys (**Figure 3a** and **Figure 9a$_1$**). The microstructures of the composites include Ti_2Cu, TiC and GONs in addition to the Widmanstätten microstructure (**Figure 9b$_1$**). Since the heat conductivity of the Ti alloys is low, the heat generated during sliding is accumulated, thus leading to the increase of the temperature. On one hand, the high temperature accelerates the oxidation of the alloy thus resulting in the exfoliation of the oxides (**Figure 9a$_2$**). On the other hand, the high temperature causes the softening of the alloy, thus leading to the enlargement of the contact area under the same load. Besides, under the locally and instantaneously high temperature at the contact asperities, the hard protrusions at the surface of the Si_3N_4 ball and its severe penetration into the soft matrix leave significant furrows on the sample surface and remove some materials in the grooves (**Figure 9a$_2$**). All these factors cause the increase of the wear volume loss and reduce the wear resistance of the Ti alloy.

Introducing GONs and copper to the interfaces of the TC4 powders leads to the formation of the nanoscale precipitates of Ti_2Cu and TiC during the SPS. These fine and stable precipitates act as hard obstacles to prevent dislocations' movement under the high temperature, thus resulting in the increase of the high temperature strength and reduce the contact area during sliding. The increase of strength also increases the

resistance of the composites to the formation of furrows, thus resulting in the reduction of both the groove depth and the roughness of the surface (**Figure 9b$_2$**). Furthermore, the remaining elemental copper and GONs existed at the interfaces between the matrix grains enhance the heat conduction due to their high heat conductivities. This can lower the increase rate of the temperature caused by sliding, slow down the oxidation rate, and reduce the oxide wear debris.

However, with the further increase of the content of copper, the density of the Ti_2Cu precipitates increases, thus resulting in the increase of the crack initiation probability at the interfaces between the Ti_2Cu particles and the matrix due to stress localization at these interfaces under sliding wear. Therefore, excessive amount of Ti_2Cu precipitates in the Ti matrix composites have caused a deleterious effect on the wear resistance of the composites.

Besides, the pulling-out of the GONs from the interfaces between the matrix grains separates locally the Si_3N_4 ball and the composites, preventing the direct contact and acting as a lubricant (**Figure 9b$_2$**). Furthermore, since the TiC forms *in situ* at the interface between the TC4 matrix and the GONs, the TiC and the remaining GONs are fused into a brittle structure, which is denoted as TiC@GONs here. During sliding, the brittle TiC@GONs are crushed and the TiC and GONs are separated from each other, thus reducing the local penetration depth of the abrasive asperities when in contact, finally lowering the wear rate [41]. Hence, the improvement of the tribological properties of GONs-*x*Cu/TC4 composites is mainly due to the strengthening by the nanoscale precipitates (i.e. Ti_2Cu and TiC), the fragileness of the

brittle TiC@GONs structure, and the enhanced heat conduction resulted from the high heat conductivity of the preserved elemental copper and GONs.

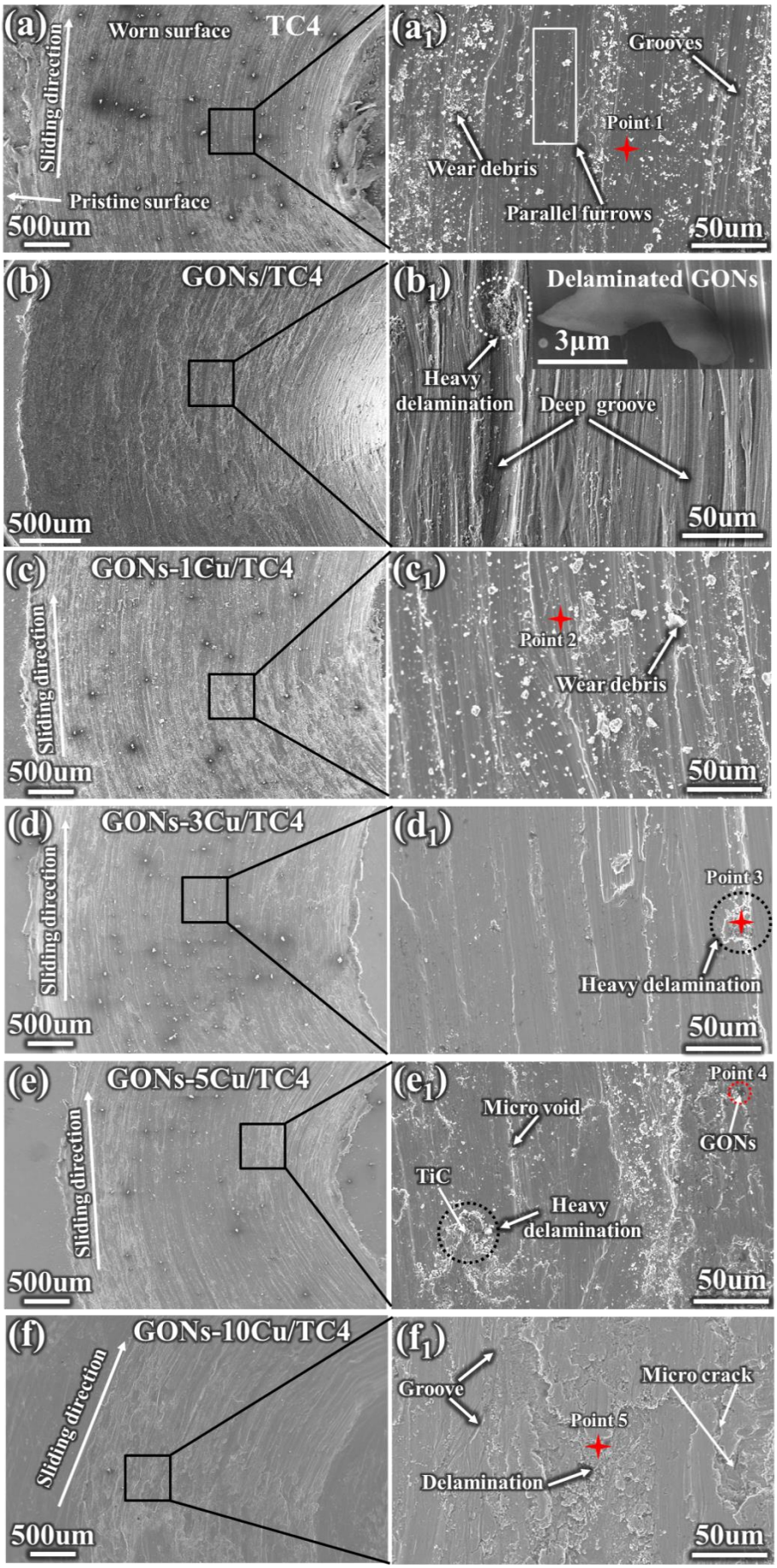
(a)
Worn surface
TC4
Sliding direction
Pristine surface
500um
(a1)
Grooves
Point 1
Wear debris
Parallel furrows
50um
(b)
GONs/TC4
500um
(b1)
Delaminated GONs
3μm
Heavy delamination
Deep groove
50um
(c)
GONs-1Cu/TC4
Sliding direction
500um
(c1)
Point 2
Wear debris
50um
(d)
GONs-3Cu/TC4
Sliding direction
500um
(d1)
Point 3
Heavy delamination
50um
(e)
GONs-5Cu/TC4
Sliding direction
500um
(e1)
Micro void
Point 4
GONs
TiC
Heavy delamination
50um
(f)
GONs-10Cu/TC4
Sliding direction
500um
(f1)
Groove
Micro crack
Point 5
Delamination
50um

1

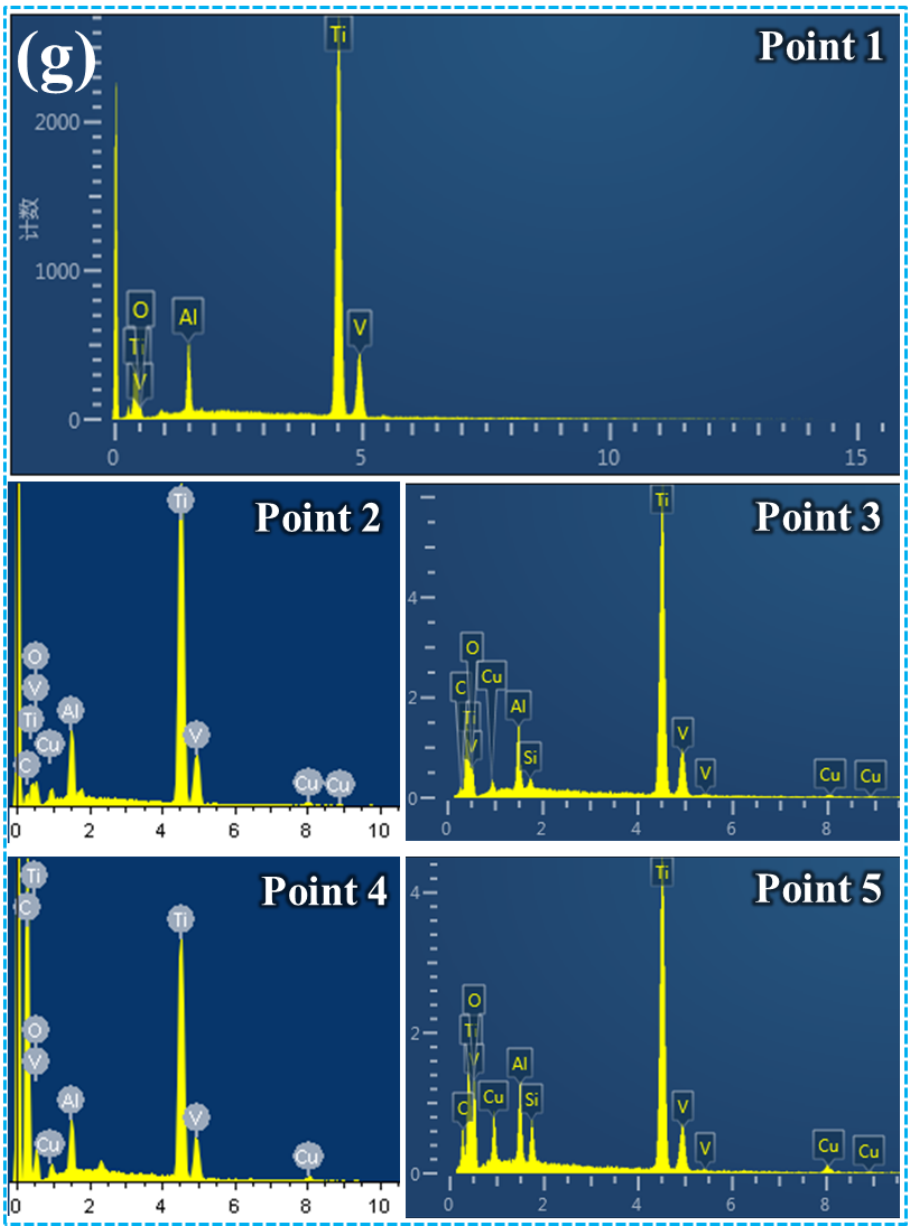

Figure 8. SEM images showing the sintered composites surface after friction test and the EDS analysis results on the worn surfaces. (a) TC4, (b) GONs/TC4, (c) GONs-Cu/TC4, (d) GONs-3Cu/TC4, (e) GONs-5Cu/TC4 and (f) GONs-10Cu/TC4, (g) corresponding to EDS analysis on point 1, 2, 3, 4 and 5 in Figure (a_1), (c_1), (d_1), (e_1), and (f_1), respectively.

Table 4. Chemical compositions (in at. %) of different positions on the worn surface in Figure 8.

Position	Ti	Al	V	O	Si	C	Cu
Point 1	61.09	5.32	3.38	30.21	0	0	0
Point 2	61.54	5.22	3.02	26.92	0.85	1.54	0.91
Point 3	58.13	5.68	1.78	20.33	1.07	12.77	0.24
Point 4	4.36	1.67	0.41	6.46	0.56	85.75	0.89
Point 5	34.26	4.17	1.04	41.21	2.07	13.58	3.67

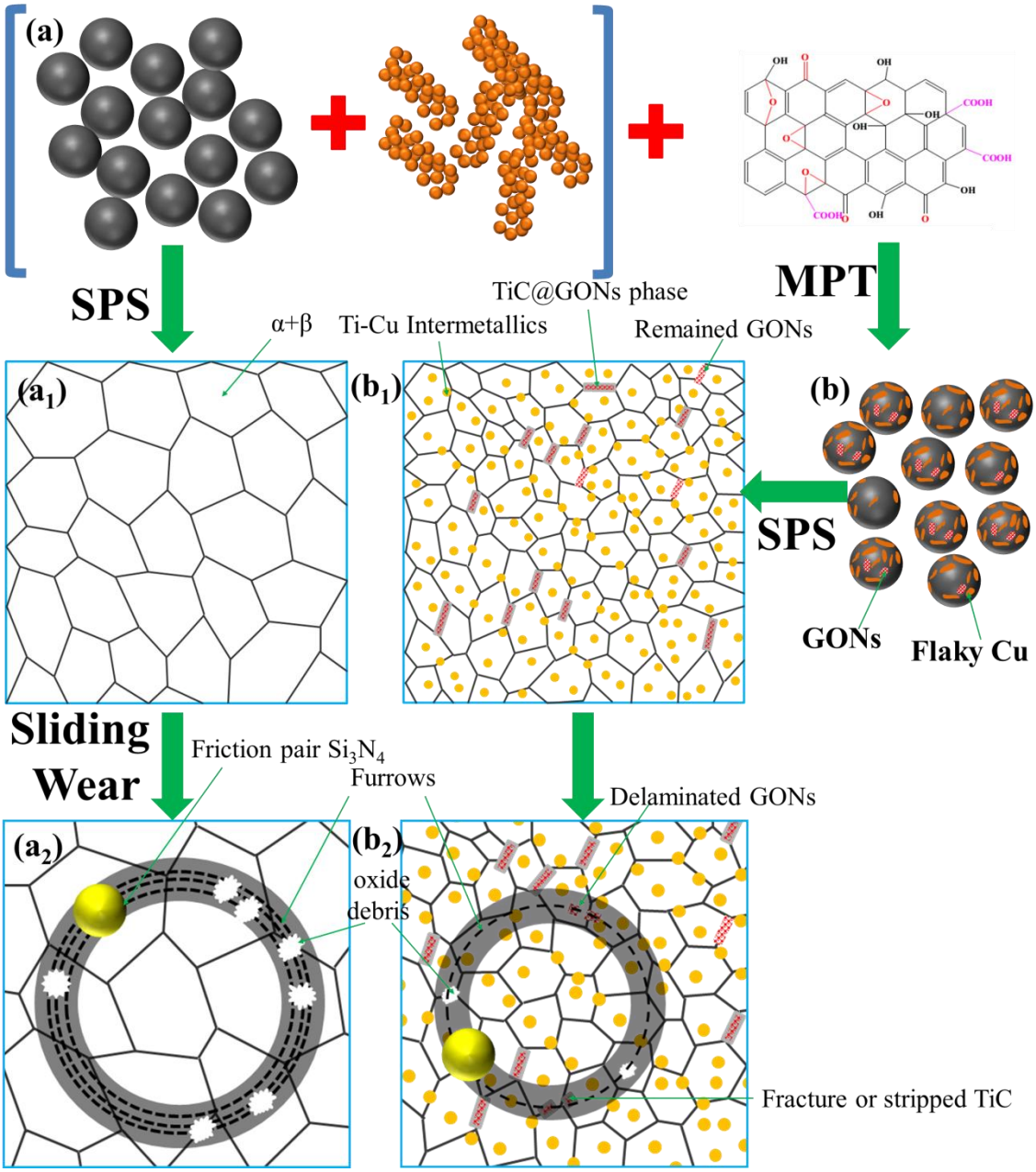

Figure 9. Schematic diagram and mechanism of tribological behavior of Ti matrix composites co-strengthen with GONs and Cu in this work. ***MPT=Modification powders technology**

4 Conclusions

In this study, powder metallurgy and SPS technology have been applied to improve the microstructure and tribological properties of TC4 matrix composites with the reinforcement of 0.3 wt% GONs and Cu. The unreacted GONs, *in-situ* formed TiC particles or layers and Ti_2Cu nanoscale precipitates were generated in the Ti matrix composites, leading to excellent hardness and tribological properties. The peak hardness (411 HV) appears at the composites with 5 wt.% copper, and it is ~25% higher than the hardness of the TC4 alloy (330 HV). The change of the coefficients of friction and the wear volume loss with the content of copper show similar trends, i.e., decreasing when the content of copper is less than 3wt.% but increasing when the concentration is larger 3 wt.%. The GONs-*x*Cu/TC4 composites show the lowest coefficients of friction (0.12) and the wear volume loss (0.155 mm^3) among the alloys and composites studied in the present work. The improvement of the tribological properties is due to the strengthening by the nanoscale precipitates (Ti_2Cu and TiC) formed at high temperatures, self-lubricating effect introduced by the pulled out GONs from the composites, the fragileness of the brittle TiC@GONs structure, and the enhanced heat conduction resulted from the high heat conductivity of the preserved elemental copper and graphene oxides.

Acknowledgement

The authors would like to acknowledge the financial support from National Natural Science Foundation of China (No. 51901192), Key Research and Development Projects of Shaanxi Province (No. 2019GY-164), Science and Technology Project of Weiyang District of Xi'an City (No. 201857), Shaanxi Youth Star Program of Science and Technology (No. 2020KJXX-061), as well as Newton Mobility Grant (No. IE161019) through Royal Society and the National Natural Science Foundation of China.

References

[1] M. Geetha, A.K. Singh, R. Asokamani, A.K. Gogia. Ti based biomaterials, the ultimate choice for orthopaedic implants-a review. Prog. Mater. Sci. 54 (2009) 397–425.

[2] S.Y. Sun, M.M. Wang, L.Q. Wang, J.N. Qin, W.J. Lu, D. Zhang. The influences of trace TiB and TiC on microstructure refinement and mechanical properties of in situ synthesized Ti matrix composite. Compos. Part B: Eng. 43 (2012) 3334–3337.

[3] C.Veiga, J.P. Davim, A.J.R. Loureiro. Properties and applications of titanium alloys: a brief review, Rev. Adv. Mater. Sci. 32 (2012) 133–148.

[4] Y. Bao, L.J. Huang, Q. An, S. Jiang, L. Geng, X.X. Ma. Wire-feed deposition TiB reinforced Ti composite coating: Formation mechanism and tribological properties, Mater. Lett. 229 (2018) 221–224.

[5] W.H. Kao, Y.L. Su, J.H. Horng, H.C. Huang, S.E. Yang. Improved tribological, electrochemical and biocompatibility properties of Ti6Al4V alloy by gas-nitriding and Ti–C:H coating. Surf. Coat. Tech. 283 (2015) 70–79.

[6] P.Q. La, J.Q. Ma, Y.T. Zhu, J. Yang, W.M. Liu, Q.J. Xue, R.Z. Valiev. Dry-sliding tribological properties of ultrafine-grained Ti prepared by severe plastic deformation.

Acta Mater. 53 (2005) 5167–5173.
[7] K. Geng, W.J. Lu, D. Zhang, T. Sakata, H. Mori. Tensile properties of in situ synthesized titanium matrix composites reinforced by TiB and Nd_2O_3 at elevated temperature. Mater. Des. 24 (2003) 409–414.
[8] L. Huang, L. Wang, M. Qian, J. Zou. High tensile-strength and ductile titanium matrix composites strengthened by TiB nanowires. Scripta Mater. 141 (2017) 133–137.
[9] J.W. Lu, Y.Q. Zhao, Y. Du, W. Zhang, Y.S. Zhang. Microstructure and mechanical properties of a novel titanium alloy with homogeneous $(TiHf)_5Si_3$ particle reinforcements. J. Alloy. Compd. 778 (2019) 115–123.
[10] Y. Liu, L.L. Dong, J.W. Lu, W.T. Huo, Y. Du, W. Zhang, Y.S. Zhang. Microstructure and mechanical properties of SiC nanowires reinforced titanium matrix composites. J. Alloy. Compd. 819 (2020) 152953.
[11] L.L. Dong, W.G. Chen, C.H. Zheng, N. Deng, Microstructure and properties characterization of tungsten-copper composite materials doped with graphene, J. Alloy. Compd. 695 (2017) 1637–1646.
[12] L.L. Dong, B. Xiao, L.H. Jin, J.W. Lu, Y. Liu, Y.Q. Fu, Y.Q. Zhao, G.H. Wu, Y.S. Zhang. Mechanisms of simultaneously enhanced strength and ductility of titanium matrix composites reinforced with nanosheets of graphene oxides. Ceram. Int. 45 (2019) 19370–19379.
[13] K. Chu, F. Wang, Y.B. Li, X.H. Wang, D.J. Huang, Z.R. Geng. Interface and mechanical/thermal properties of graphene/copper composite with Mo_2C nanoparticles grown on graphene. Compos. Part A 109 (2018) 267–279.
[14] P.Z. Shao, W.S. Yang, Q. Zhang, Q.Y. Meng, X.Tan, Z.Y. Xiu, J. Qiao, Z.H. Yu, G.H. Wu. Microstructure and tensile properties of 5083 Al matrix composites reinforced with graphene oxide and graphene nanoplates prepared by pressure infiltration method. Compos. Part A 109 (2018) 151–162.
[15] K. Chu, J. Wang, Y.P. Liu, Z.R. Geng. Graphene defect engineering for optimizing the interface and mechanical properties of graphene/copper composites. Carbon 140 (2018) 112–123.

[16] Y. Wu, K. Zhan, Z. Yang, W. Sun, B. Zhao, Y. Yan, J. Yang. Graphene oxide/Al composites with enhanced mechanical properties fabricated by simple electrostatic interaction and powder metallurgy. J. Alloy. Compd. 775 (2019) 233–240.

[17] L.L. Dong, B. Xiao, Y. Liu, Y.L. Li, Y.Q. Fu, Y.Q. Zhao, Y.S. Zhang. Sintering effect on microstructural evolution and mechanical properties of spark plasma sintered Ti matrix composites reinforced by reduced graphene oxides. Ceram. Int. 44(15) (2018) 17835–17844.

[18] X.N. Mu, H.N. Cai, H.M. Zhang, Q.B. Fan, F.C. Wang, Z.H. Zhang, Y.X. Ge, R. Shi, Y. Wu, Z. Wang, D.D. Wang, S. Chang. Uniform dispersion and interface analysis of nickel coated graphene nanoflakes/pure titanium matrix composites. Carbon 137 (2018) 146-155.

[19] J.L. Murray. The Cu-Ti system. Bulletin of alloy phase diagrams, 4. Metals Park. OH: ASM International, 1983 4 81-95.

[20] C. Peng, Y. Liu, H. Liu, S.Y. Zhang, C.G. Bai, Y.Z. Wan, L. Ren, K. Yang. Optimization of annealing treatment and comprehensive properties of Cu-containing Ti6Al4V-*x*Cu alloys. J. Mater. Sci. Technol. 35(2019) 2121–2131.

[21] H. Wei, L.F. Hou, Y.C. Cui, Y.H. Wei. Effect of Ti content on corrosion behavior of Cu-Ti alloys in 3.5% NaCl solution. T. Nonferr. Metal. Soc. 28 (2018) 669-675.

[22] H. Wei, Y.H. Wei, L.F. Hou, N. Dang. Correlation of ageing precipitates with the corrosion behaviour of Cu-4wt.% Ti alloys in 3.5 wt.% NaCl solution. Corros. Sci. 111(2016) 382-390.

[23] M. Kikuchi, Y. Takada, S. Kiyosue, M. Yoda, M. Woldu, Z. Cai, O. Okuno, T. Okabe. Mechanical properties and microstructures of cast Ti-Cu alloys. Dent. Mater. 19(2003) 174-181.

[24] B. Mei, Y. Miyamoto, Preparation of Ti-Al intermetallic compounds by spark plasma sintering, Metall. Mater. Trans. A 32 (2001) 843–847.

[25] L. Gao. Spark plasma sintering technology, J. Inorg. Mater. 12 (1997) 129–133.

[26] R.M. German. Sintering densification for powder mixtures of varying distribution widths. Acta Metall. Sin. 40 (1992) 2085–2089.

[27] L.L. Dong, W.G. Chen, N. Deng, C.H. Zheng. A novel fabrication of graphene by

chemical reaction with a green reductant. Chem. Eng. J. 306 (2016) 754–762.
[28] L.J. Huang, L. Geng, H.X. Peng, B. Kaveendran. High temperature tensile properties of in situ TiB_w/Ti6Al4V composites with a novel network reinforcement architecture. Mater. Sci. Eng. A 534 (2012) 688– 692.
[29] L.L. Dong, J.W. Lu, Y.Q. Fu, W.T. Huo, Y. Liu, D.D. Li, Y.S. Zhang. Carbonaceous nanomaterial reinforced Ti-6Al-4V matrix composites: Properties, interfacial structures and strengthening mechanisms. Carbon 164 (2020) 272–286.
[30] J.W. Lu, L.L. Dong, Y. Liu, Y.Q. Fu, W. Zhang, Y. Du, Y.S. Zhang, Y.Q. Zhao. Simultaneously enhancing the strength and ductility in titanium matrix composites via discontinuous network structure. Compos. Part A 136 (2020) 105971.
[31] Y.H. Liang, H.Y. Wang, Y.F. Yang, Y.Y. Wang, Q.C. Jiang, Evolution process of the synthesis of TiC in the Cu-Ti-C system, J. Alloy. Compd. 452 (2008) 298-303.
[32] M. Kikuchi, Y. Takada, S. Kiyosue, M. Yoda, M. Woldu, Z. Cai, O. Okuno, T. Okabe. Mechanical properties and microstructures of cast Ti–Cu alloys. Dent. Mater. 19(3) (2003) 174–181.
[33] J.T. Robinson, F.K. Perkins, E.S. Snow, Z.Q. Wei, P.E. Sheehan. Reduced graphene oxide molecular sensors. Nano Lett. 8 (10) (2008) 3137–3140.
[34] K.S. Munir, M. Qian, Y.C. Li, D.T. Oldfield, P. Kingshott, D.M. Zhu, C. Wen. Quantitative analyses of MWCNT-Ti powder mixtures using raman spectroscopy: the influence of milling parameters on nanostructural evolution. Adv. Eng. Mater. 17(11) (2015) 1660–1669.
[35] J.W. Hwang, T.S. Yoon, S.H. Jin, J.S. Lee, T.S. Kim, S.H. Hong. Enhanced mechanical properties of graphene/copper nanocomposites using a molecularlevel mixing process. Adv. Mater. 2013, 25, 6724–6729.
[36] C. Ohkubo, I. Shimura, T. Aoki, S. Hanatani, T. Hosoi, M. Hattori, Y. Oda, T. Okabe. Wear resistance of experimental Ti-Cu alloys. Biomaterials 24 (2003) 3377–3381.
[37] D.D. Gu, Y.C. Hagedorn, W. Meiners, K. Wissenbach, R. Poprawe. Nanocrystalline TiC reinforced Ti matrix bulk-form nanocomposites by Selective Laser Melting (SLM): Densification, growth mechanism and wear behavior. Compos.

Sci. Technol. 71 (2011) 1612–1620.
[38] G. Li, S.G. Qu, Y.X. Pan, X.Q. Li. Effects of the different frequencies and loads of ultrasonic surface rolling on surface mechanical properties and fretting wear resistance of HIP Ti–6Al–4V alloy. Appl. Surf. Sci. 389 (2016) 324–334.
[39] A.S. Namini, S.A.A. Dilawary, A. Motallebzadeh, M. Shahedi Asl. Effect of TiB_2 addition on the elevated temperature tribological behavior of spark plasma sintered Ti matrix composite. Compos. Part B 172 (2019) 271–280.
[40] A. Wei-YeeTan, J.Y. Lek, W. Sun, A. Bhowmik, I. Marinescu, P.J. Buenconsejo, Z.L. Dong, E.J. Liu. Microstructure, mechanical and tribological properties of cold sprayed Ti6Al4V–CoCr composite coatings. Compos. Part B 202 (2020) 108280.
[41] M.W. Bai, R. Namus, Y.D. Xu, D.K. Guan, M.W. Rainforth, B.J. Inkson. *In-situ* Ti-6Al-4V/TiC composites synthesized by reactive spark plasma sintering: processing, microstructure, and dry sliding wear behavior. Wear 432–433 (2019) 202944.